KELDYSH INSTITUTE OF APPLIED MATHEMATICS
RUSSIAN ACADEMY OF SCIENCES

A.I. Neishtadt, V.V. Sidorenko

WISDOM SYSTEM: DYNAMICS IN THE ADIABATIC APPROXIMATION

MOSCOW
2003

A.I.Neishtadt, V.V.Sidorenko

Wisdom system: dynamics in the adiabatic approximation

The Wisdom system is the Hamiltonian system with two degrees of freedom constructed as a simple approximate model describing some properties of the asteroid motion over long time scales. Its Hamiltonian is the principal part of the Hamiltonian of the planar elliptic restricted three body problem, averaged under the assumption of 3:1 mean-motion resonance. The phase variables of the Wisdom system evolve at different rates and can be subdivided into the "fast" and "slow" ones. Important feature of this system is the existence of an approximate integral, adiabatic invariant. We present detailed classification of the slow variables' evolution paths. We also consider properties of the adiabatic chaos area arising in the system's phase space. It emerges as a result of the adiabatic invariance violations generated by qualitative changes in the behavior of fast variables. In particular, numerous stable long-periodic solutions are revealed.

А.И.Нейштадт, В.В.Сидоренко

Система Уиздома: динамика в адиабатическом приближении

Системой Уиздома называют гамильтонову систему с двумя степенями свободы, порождаемую главной частью гамильтониана плоской ограниченной эллиптической задачи трех тел, усредненного в предположении резонанса средних движений 3 : 1. Динамика системы Уиздома характеризуется разделением переменных на «быстрые» и «медленные» и наличием приближенного интеграла – адиабатического инварианта. В статье дана подробная классификация возможных вариантов эволюции «медленных» переменных. Отмечается существование многочисленных устойчивых периодических движений в области адиабатического хаоса, возникающей в результате нарушений адиабатичности при изменении качественного поведения «быстрых» переменных.

Introduction

Twenty years ago J.Wisdom undertook extensive investigation of the long-term evolution of asteroid distribution near the 3:1 mean-motion resonance with Jupiter [1, 2, 3]. His studies were substantially based on the asteroid dynamics analysis in the frames of the elliptic planar restricted three body problem: Sun - Jupiter - asteroid. It turned out that in the main approximation the Hamiltonian of this problem, being averaged over the asteroid's and Jupiter's mean longitudes near the resonance, acquires a rather simple structure: "fast" and "slow" phase variables emerge and, at fixed values of the "slow" variables, the Hamiltonian becomes identical to that of the mathematical pendulum.

A two degrees of freedom Hamiltonian system, described by the truncated Hamiltonian, will hence be called the "Wisdom systems". This system is of interest not only due to its significant role in the Wisdom theory of the 3:1 Kirkwood gap. It can also be used as a convenient model for investigation of resonant motions at small values of the asteroid's eccentricity e, of Jupiter's eccentricity e_J, and of its part μ_J in the total system's mass.

We intend to present some results on the general properties of the Wisdom system. We have explored its dynamics on different levels of H_W, where H_W is the system's Hamiltonian (the Wisdom Hamiltonian). Existence of qualitative distinctions was mentioned in [3], but a detailed description of all possible scenarios for the slow variable evolution has never been presented so far.

A special attention is paid to the region of the so-called "adiabatic" chaos in the system's phase space. Small quasi-random jumps of the "fast" subsystem's adiabatic invariant result in scattering of trajectories in this region [4, 5]. The jumps may also produce a qualitative change of the motion in the system. In some cases this phenomenon can entail sudden increase of the resonant asteroid eccentricity. According to Wisdom's hypothesis, this effect is responsible for the formation of the 3:1 Kirkwood gap.

As follows from the arguments presented in [6], the region of the "adiabatic" chaos is the area of co-existence of the regular and chaotic dynamics. This domain contains a lot of stable periodic trajectories surrounded by stability islands. The total measure of these islands does not tend to 0 for $\varepsilon \to 0$, where

$$\varepsilon = \frac{\mu_J^{1/2}}{e_J} \sim \frac{T_f}{T_s} \ll 1,$$

T_f and T_s being the typical timescales of the fast and slow motions in Wisdom's system.

Numeric modelling confirms the presence of numerous stable periodic trajectories in the mentioned domain of the phase space.

In the present paper we concentrate on the Wisdom system itself and avoid whatever conclusions related to the asteroids' dynamics at 3:1 resonance. To

apply our results to this dynamics, it would be necessary to carefully analyze to what extent the Wisdom system can serve as a model of the elliptic planar reduced three body problem. Some remarks concerning the limited applicability of the Wisdom model can be found in [7, 8].

1. Definition of the Wisdom system.

According to [1], in the main approximation, the secular evolution of the asteroid motion in 3:1 resonance with Jupiter is described by the canonical equations

$$\dot{\varphi} = \{\varphi, H_W\},\ \dot{\Phi} = \{\Phi, H_W\}, \tag{1.1}$$
$$\dot{x} = \{x, H_W\},\ \dot{y} = \{y, H_W\}.$$

Here φ is the critical angle (three times the mean longitude of Jupiter minus the mean longitude of the asteroid), Φ is some function of the asteroid's semimajor axis a, x and $-y$ are proportional to the Laplace vector components

$$x \approx a^{1/4}\left(\frac{e}{e_j}\right)\cos\omega,\ y \approx -a^{1/4}\left(\frac{e}{e_j}\right)\sin\omega,$$

with ω being the longitude of the asteroid perihelion.

The Poisson brackets $\{\cdot,\cdot\}$ in (1.1) are defined in such a way that

$$\{\varphi, \Phi\} = 1,\ \{x, y\} = \varepsilon,$$

$$\{\varphi, x\} = \{\varphi, y\} = \{\Phi, x\} = \{\Phi, y\} = 0.$$

To bring the evolutionary equations into the form (1.1), the expression for the Hamiltonian H_W, given by Wisdom in [1], should be rewritten as follows:

$$H_W(\varphi, \Phi, x, y) = \frac{1}{2}\alpha\Phi^2 + [C(x^2 - y^2) + Dx + E]\cos\varphi + \tag{1.2}$$
$$+ y(2Cx + D)\sin\varphi - [F(x^2 + y^2) + Gx].$$

The values of the coefficients α, C, D, E, F, G depend on the resonant value of the asteroid's semimajor axis $a_{res} = \sqrt[3]{(1-\mu_J)/9}$. Using the formulae developed in [1], we obtain at $a_{res} = 3^{-2/3} \approx 0.48074986$ (which is the limit value of a_{res} at μ_J goes to 0):

$$\alpha \approx 12.98024613,\ C \approx 0.86355748,\ D \approx -2.65764714,$$

$$E \approx 0.36337472,\ F \approx -0.20514373,\ G \approx 0.19889968.$$

In [1] these coefficients were evaluated at $a_{res} \approx 0.48059680$ ($\mu_J = 1/1047.355$).

Separating the terms that depend on φ, Φ from the terms that are independent from these variables, we get

$$H_W = H_0(\varphi, \Phi, x, y) + H_1(x, y). \tag{1.3}$$

The function $H_0(\varphi, \Phi, x, y)$ at fixed x, y is the Hamiltonian of a pendulum:

$$H_0(\varphi, \Phi, x, y) = \frac{1}{2}\alpha\Phi^2 - A(x, y)\cos(\varphi - R(x, y)). \tag{1.4}$$

Here

$$\operatorname{tg} R(x, y) = \frac{y(2Cx + D)}{C(x^2 - y^2) + Dx + E},$$

$$A(x, y) = \left\{ \left[C(x^2 - y^2) + Dx + E \right]^2 + y^2(2Cx + D)^2 \right\}^{1/2}.$$

As it was noted in [9], the coefficient $A(x, y)$ is the product of the distances in $\mathbf{R}^2$ from the point (x, y) to points $P_1 = (x_1, 0)$ and $P_2 = (x_2, 0)$, where

$$x_1 = -\frac{D + \sqrt{D^2 - 4CE}}{2C} \approx 0.14341,$$

$$x_2 = -\frac{D - \sqrt{D^2 - 4CE}}{2C} \approx 2.93415.$$

The second term in (1.3) is

$$H_1(x, y) = -F(x^2 + y^2) + Gx.$$

Surprisingly, the Hamiltonian H_W is independent from the Jupiter's eccentricity e_J. This parameter defines the values and the typical timescale of the secular changes of the asteroid orbital elements. Nevertheless, if the Jupiter's eccentricity is non-zero and small enough, in the main approximation its value does not affect the topological phase flow properties of the planar elliptic three body problem averaged at the resonance.

It is important to mention the reversibility of the system (1.1): if

$$\mathbf{z}(t) = (\varphi(t),\ \Phi(t),\ x(t),\ y(t))^T$$

is its solution, then

$$\mathbf{z}_*(t) = Q\mathbf{z}(-t),\ Q = \operatorname{diag}(-1, 1, 1, -1),$$

is also a solution. This property was used for numerical search for periodic solutions (**Sec. 4**).

Table 1. The relation between ε and μ_J values
for the case of Jupiter's motion in orbit of eccentricity $e_J = 0.048$

ε	μ_J
0.2	$9.2 \cdot 10^{-5}$
0.1	$2.3 \cdot 10^{-5}$
0.05	$5.8 \cdot 10^{-6}$
0.025	$1.4 \cdot 10^{-6}$

The Table 1 provides an insight into the values of the three body problem parameters e_J, μ_J and the related values of the Wisdom system parameter ε. The accepted value of Jupiter's eccentricity ($e_J = 0.048$) is conventional for model calculations in the asteroidal dynamics.

2. Adiabatic approximation

In general, the phase variables φ, Φ, x, y evolve at different rates: φ, Φ are the "fast" variables ($\dot{\varphi}, \dot{\Phi} \sim 1$), x, y are the "slow" variables ($\dot{x}, \dot{y} \sim \varepsilon$). Below, the equations describing the behavior of the fast variables will be called "the fast subsystem". The slow subsystem will be constituted by the equations for the slow variables, respectively.

2.1. Properties of the fast subsystem

At $\varepsilon = 0$ the fast subsystem dynamics is described by the mathematical pendulum equations

$$\dot{\varphi} = \alpha\Phi, \ \dot{\Phi} = -A(x,y)\sin(\varphi - R(x,y)), \tag{2.1}$$

where x, y should be considered as parameters. The phase portrait of the subsystem (2.1) is given by Fig.1. The separatrices separate the regions of oscillatory and rotational behavior of the critical angle φ.

Let $\varphi(t,x,y,h), \Phi(t,x,y,h)$ denote the solution of equations (2.1) at fixed values of x, y satisfying the condition

$$H_W(\varphi(t,x,y,h), \Phi(t,x,y,h), x, y) = h.$$

Its qualitative behavior depends on the value of the parameter

$$\kappa = \frac{1}{\sqrt{2}}\left(1 + \frac{h - H_1(x,y)}{A(x,y)}\right)^{1/2}.$$

The angle φ oscillates in the case $\kappa < 1$, and rotates at $\kappa > 1$. The separatrices correspond to $\kappa = 1$.

In subsystem (2.1), we can introduce new variables

$$I = I(h, x, y), \chi = \chi(\varphi, \Phi, x, y).$$

For the rotational solutions, $I, \chi \bmod 2\pi$ coincide with the "action-angle" variables, while for the oscillating solutions I is a half of the "action" variable value and $\chi \bmod 4\pi$ is equal to the doubled value of the "angle" variable. This change of the variables is the canonical transformation with some generating function $W(\varphi, I, x, y)$, where x, y should again be considered as parameters.

In the case $\varepsilon \neq 0$, equations (2.1) describe the dynamics of a pendulum with slowly varying parameters. Away from the separatrices, $I(h, x, y)$ is the adiabatic invariant of the Wisdom system. Along the solutions of equations (1.1), its value is preserved with the accuracy of $O(\varepsilon)$ over the time interval of order $1/\varepsilon$.

2.2. Properties of the slow subsystem

To study the qualitative behavior of the slow variables x, y we perform the canonical transformation

$$(\varphi, \Phi, x, y) \mapsto (\overline{\chi}, \overline{I}, \overline{x}, \overline{y}), \tag{2.2}$$

the relations between the new and old variables being

$$\overline{\chi} = \frac{\partial W}{\partial \overline{I}}(\varphi, \overline{I}, x, \overline{y}),\ \Phi = \frac{\partial W}{\partial \varphi}(\varphi, \overline{I}, x, \overline{y}), \tag{2.3}$$

$$\overline{x} = x + \varepsilon \frac{\partial W}{\partial \overline{y}},\ y = \overline{y} + \varepsilon \frac{\partial W}{\partial x}.$$

As it follows from formulae (2.3), this transformation is close to the identical one on variables x, y. After transformation (2.2), the symplectic structure in the Wisdom system's phase space is defined by the Poisson brackets with the following values

$$\{\overline{\chi}, \overline{I}\} = 1,\ \{\overline{x}, \overline{y}\} = \varepsilon,$$
$$\{\overline{\chi}, \overline{x}\} = \{\overline{\chi}, \overline{y}\} = \{\overline{I}, \overline{x}\} = \{\overline{I}, \overline{y}\} = 0.$$

The Wisdom Hamiltonian admits the form

$$\Xi(\overline{\chi}, \overline{I}, \overline{x}, \overline{y}) = \Lambda_W(\overline{I}, \overline{x}, \overline{y}) + O(\varepsilon).$$

Here $\Lambda_W(I, x, y)$ is the Hamiltonian H_W rewritten as a function of I, x, y.

If the projection of the phase point $\mathbf{z(t)}$ onto the phase portrait of the frozen fast subsystem is away from the separatrices, the evolution of the slow variables $\overline{x}, \overline{y}$ is described, with the accuracy of $O(\varepsilon)$ over time intervals of order $1/\varepsilon$, by the equations

$$\dot{\overline{x}} = \varepsilon \frac{\partial \Lambda_W}{\partial \overline{y}}(\overline{I}, \overline{x}, \overline{y}),\ \dot{\overline{y}} = -\varepsilon \frac{\partial \Lambda_W}{\partial \overline{x}}(\overline{I}, \overline{x}, \overline{y}), \tag{2.4}$$

where $\overline{I}$ should be considered as a fixed parameter. This statement remains valid after the formal substitution of the initial variables x, y and $I(h, x(0), y(0))$ instead of $\overline{x}, \overline{y}, \overline{I}$. Therefore we shall omit the dash over the evolutionary variables below.

Taking into account relation (1.3), we obtain

$$\Lambda_W(I, x, y) = \Lambda_0(I, x, y) + H_1(x, y), \tag{2.5}$$

where $\Lambda_0(I, x, y)$ is the Hamiltonian H_0 expressed in terms of I, x, y. Writing H_0 as a composite function

$$H_0(\varphi, \Phi, x, y) = H_0(\varphi, \Phi, A(x, y), R(x, y)),$$

we get

$$\Lambda_0(I, x, y) = \Lambda_0(I, A(x, y)). \tag{2.6}$$

Now let us differentiate with respect to A the left-hand and the right-hand sides of the equality

$$I = \frac{1}{2\pi} \int_{\varphi_*}^{\varphi^*} \left[\frac{2}{\alpha} \left(\Lambda_0(I, A) + A \cos(\xi - R) \right) \right]^{1/2} d\xi,$$

where φ_*, φ^* are functions of I, A, R. After some manipulations with these formulae, one can find

$$\frac{\partial \Lambda_0}{\partial A}(I, A(x, y)) = \langle \cos(\varphi - R) \rangle. \tag{2.7}$$

The angle brackets in (2.7) denote averaging over χ:

$$\langle f(\varphi, x, y) \rangle = \frac{1}{2\pi\sigma} \int_0^{2\pi\sigma} f(\varphi(\chi, I, x, y), x, y)\, d\chi.$$

Here $\sigma = 1$ if the function $\varphi(\chi, I, x, y)$ corresponds to the rotational motion in the fast subsystem; in the case of averaging over the oscillatory solution $\sigma = 2$.

Explicit expressions for $\langle\cos(\varphi - R)\rangle$ were given in [3]. Using our notations, we have

$$\langle\cos(\varphi - R)\rangle = \begin{cases} 2\kappa^2 \dfrac{E\left(\dfrac{1}{\kappa}\right)}{K\left(\dfrac{1}{\kappa}\right)} + 1 - 2\kappa^2, & \kappa > 1 \\ \dfrac{2E(\kappa)}{K(\kappa)} - 1, & \kappa < 1 \end{cases} \tag{2.8}$$

In these formulae $K(\cdot)$ and $E(\cdot)$ denote the complete elliptic integrals of the first and second kinds, respectively.

Relations (2.5)-(2.7) allow us to rewrite equations (2.4) as follows:

$$\dot{x} = \varepsilon \left(\frac{\partial H_1}{\partial y} + \frac{\partial A}{\partial y} \langle\cos(\varphi - R)\rangle \right), \tag{2.9}$$

$$\dot{y} = -\varepsilon \left(\frac{\partial H_1}{\partial x} + \frac{\partial A}{\partial x} \langle\cos(\varphi - R)\rangle \right).$$

Substituting (2.8) into system (2.9) we obtain the evolutionary equations describing the long-term dynamics of the slow subsystem at the level $H_W = h$.

2.3. Forbidden area and uncertainty curve

Let

$$h_*(x, y) = H_1(x, y) - A(x, y),\ h^*(x, y) = H_1(x, y) + A(x, y).$$

The region $M(h) = \{x, y : h_*(x, y) > h\}$ on the plane x, y is the forbidden area for the phase trajectories of the system (2.9): for a given value of h, slow variables can not accept values from $M(h)$.

The curve $\Gamma(h) = \{x, y : h^*(x, y) = h\}$ is called the uncertainty curve. In the case $h^*(x, y) = h$ the trajectory in the fast subsystem (at fixed x, y) is a separatrix. Consequently, here the adiabatic approximation loses its validity. Dependent upon the value of h, the curve $\Gamma(h)$ consists of one or two ovals or does not exist at all (**Sec.3**). If one takes x, y from the region bounded by the curve $\Gamma(h)$ ($h > h^*(x, y)$), the critical angle φ rotates in the solutions of the system (1.1) on the level $H_W = h$. For x, y selected outside of this region ($h < h^*(x, y)$), the dynamics of the fast subsystem is oscillatory.

Whenever the projection of the Wisdom system's phase trajectory on the plane x, y intersects the curve $\Gamma(h)$, the adiabatic invariant undergoes a quasi-random change [3, 4, 5]. Investigating the motion evolution over the time interval of order $1/\varepsilon$, we can neglect this violation of the adiabatic invariance:

with the accuracy of $O(\varepsilon)$ the behavior of slow variables, for the majority of initial conditions, is described by the solutions of the averaged system (2.9) matched at the uncertainty curve in accordance with the condition

$$I_{in} = I_{out}, \tag{2.10}$$

where I_{in} and I_{out} are the values of $I(h, x, y)$ along the parts of the phase trajectory of (2.9) lying inside and outside of the region bounded by the curve $\Gamma(h)$.

In the case of multiple passages across the uncertainty curve, the summing of the quasi-random changes gives rise to a diffusion of the adiabatic invariant. In particular, if we consider the behavior of the solutions $\mathbf{z}_1(t)$ and $\mathbf{z}_2(t)$ with the close initial values ($|\mathbf{z}_1(0) - \mathbf{z}_2(0)| \sim \varepsilon$), then the difference between the adiabatic invariants' values along these solutions and the difference between the projections of the phase points on the plane x, y can grow up to values of order 1 over time intervals ranging from $1/\varepsilon^2$ through $1/\varepsilon^3$ (respectively, the amount of passages performed across the uncertainty curve ranges from $\sim 1/\varepsilon$ to $\sim 1/\varepsilon^2$) [4, 5]. Quasi-random jumps of the adiabatic invariant, caused by qualitative changes in the fast motion properties, lead to formation of an adiabatic chaos region in the Wisdom system's phase space (**Sec. 3**).

3. "Slow" dynamics of Wisdom system at adiabatic approximation

Up to notations, the averaged equations (2.9) coincide with the evolutionary equations obtained by Wisdom in [3]. Comparison of the phase portraits presented in [3] reveals substantial differencies in the phase trajectories behavior at various values of the parameter h. This motivated us to explore in what way the qualitative properties of the solutions to system (2.9) depend upon h. Here we present the main results of this analysis.

3.1. Phase portraits of the slow motions

Consideration of the phase portrait of system (2.9) is the most direct way to get a clear idea of the slow motion properties at different levels $H_W = h$. It turns out that by matching (or "gluing") the trajectories at $\Gamma(h)$, in accordance with the condition $I_{in} = I_{out}$, we obtain 9 types of phase-behavior modes

structurally stable under sufficiently small variations of h. Bifurcations take place when h accepts one of the following values:

$$h_1 \approx -1.545,\ h_2 \approx -0.024,\ h_3 \approx 0.595,\ h_4 \approx 0.608,$$

$$h_5 \approx 0.612,\ h_6 \approx 1.182,\ h_7 \approx 1.932,\ h_8 \approx 3.694.$$

Brief classification of the phase portrait features is given below.

Type I: $h < h_1$. The center of the phase portrait is occupied by the "forbidden" area $M(h)$. The phase trajectories are the closed curves encircling $M(h)$. The equilibrium solutions are absent. As an example, we present in Fig. 2 the phase portrait of the slow motion at $h = -2$.

Type II: $h \in (h_1, h_2)$. The phase portrait of this type is shown in Fig. 3. After the bifurcation at $h = h_1$, the "forbidden" area consists of two domains. In addition to this, an unstable equilibrium emerges on the axis Ox. When $h \to h_1$, the equilibrium solution tends to the point $P_H = (x_H, 0)$, where

$$x_H = -\frac{D - G}{2(C - F)} \approx 1.33646.$$

At $h \to h_2$ the "forbidden" domain located in the vicinity of the coordinate origin shrinks to the point P_1.

Type III: $h \in (h_2, h_3)$. Due to the bifurcation at $h = h_2$, the uncertainty curve $\Gamma(h)$ appears on the phase portrait (Fig. 4). The curve $\Gamma(h)$ encircles the point P_1 and shrinks to it when $h \to h_2$. When the projection of the Wisdom system's phase point on the plane x, y lies inside the area bounded by the curve $\Gamma(h)$, the critical angle φ rotates. The bifurcation at $h = h_2$ also generates three additional equilibrium solutions.

Type IV: $h \in (h_3, h_4)$. At $h = h_3$, the closest to the forbidden area unstable equilibrium transforms into a stable equilibrium and a pair of unstable equilibria lying outside the Ox axis (Fig. 5).

Type V: $h \in (h_4, h_5)$. At $h = h_4$ the re-connection of the separatrices takes place (Fig. 6).

Type VI: $h \in (h_5, h_6)$. The bifurcation at $h = h_5$ results in the disappearance of the homoclinic contour pertaining to the Type V phase portraits: stable and unstable equilibria merge and vanish after that. Main features of this type of behavior are presented in Fig. 7. At $h \to h_6$ the "forbidden" area shrinks to the point P_2.

Type VII: $h \in (h_6, h_7)$. The bifurcation at $h = h_6$ resembles to some extent the bifurcation at $h = h_2$: the "forbidden" area vanishes, one more component of the uncertainty curve $\Gamma(h)$ and one more triad of equilibrium solutions appear in the vicinity of the point P_2. Two of the newly born equilibria are placed so close to each other that it is impossible to distinguish between them

on the Type VII phase portrait in Fig. 8, where they are "represented" by the same point lying on the right component of the curve $\Gamma(h)$. The enlarged fragment in Fig. 9 shows the unstable equilibrium outside the region bounded by $\Gamma(h)$ and the stable equilibrium inside it. Being so close, for all values of h taken from the interval under consideration, at $h \to h_7$ these equilibria meet at the point $P_S = (x_S, 0)$, where

$$x_S = -\frac{D+G}{2(C+F)} \approx 1.86718.$$

Type VIII: $h \in (h_7, h_8)$. An example of Type VIII phase portrait is presented in Fig. 10. At $h = h_7$ the components of the uncertainty curve connect at the point P_S. Two close equilibria pertaining to the Type VII phase portraits merge at the same point and disappear thereafter.

Type IX: $h > h_8$. At $h = h_8$ unstable equilibria (which appeared at $h = h_3$ and located outside the Ox axis till $h < h_8$) merge with the stable equilibrium lying on that axis left to the coordinate origin. So for $h > h_8$ the system (2.9) has only three equilibrium solutions: two stable equilibria and one unstable.

3.2. Bifurcation diagram

The diagram in Fig. 12 brings additional information about the phase-portrait transformations at the parameter h variation. It presents the location and the stability properties of the equilibrium solutions lying on the Ox axis.

The curve H in Fig. 12 represents the family of equilibrium solutions being born at $h = h_1$ at the point P_H. The curves S_1 and S_2 depict the families of the equilibria vanishing at $h = h_7$ in the point P_S. The notation used emphasizes the relation of these families to the periodic solutions of the three body problem found by Hill and Sinclair.

Indeed, the limit points P_H and P_S are associated in a natural way with the equilibrium solutions of the original system (1.1)

$$\varphi \equiv 0,\ \Phi \equiv 0,\ x \equiv x_H,\ y \equiv 0 \tag{3.1}$$

and

$$\varphi \equiv \pi,\ \Phi \equiv 0,\ x \equiv x_S,\ y \equiv 0. \tag{3.2}$$

When the Wisdom system provides a reasonable approximation of the three body problem dynamics, its equilibria correspond to the periodic solutions of that problem in which the asteroid rotates around the Sun three times faster than Jupiter. As it was shown in [12], the equilibrium solutions (3.1) and (3.2)

can be interpreted as analogs to the Hill solution (Jupiter's and asteroid's longitudes of the perihelion coincide) and of the Sinclair solution (the said longitudes differ in π), respectively. Detailed numerical investigations of the Hill and Sinclair solutions were undertaken in [8, 13, 14].

Finally, we would dwell upon some subtle features of the revealed chain of bifurcations. First, the attention should be drawn to the series of bifurcations for sufficiently small h variation, as shown in Fig. 13. Another remarkable property is the presence of very closely placed equilibria on the Type VII phase portraits (at a distance $\sim 10^{-3}$).

4. Long-periodic solutions

4.1. Adiabatic chaos region and stability islands

In the neighborhood of the uncertainty curve the projection of the system (1.1) phase point to the x, y plane jumps in a quasi-random way from one trajectory of the averaged system (2.9) to another: $|I_{in} - I_{out}| \sim \varepsilon$. As a result, over the long time interval this projection travels through the region $\Xi(h)$ obtained by the junction of all the slow trajectories crossing $\Gamma(h)$. The region $\Xi(h)$ consists of one or two domains. The number of domains depends on the curve $\Gamma(h)$ (Fig. 14).

Further we consider the region

$$\Xi^*(h) = \{\varphi, \Phi, x, y : H_W(\varphi, \Phi, x, y) = h, (x, y) \in \Xi(h)\}$$

in the Wisdom system's phase space. If the phase trajectory of the system (1.1) belongs to $\Xi^*(h)$, then its projection onto the x, y plane lies in the region $\Xi(h)$. The violation of adiabatic invariance, caused by the qualitative change of the fast motion character, is the main source of the trajectories' complex behavior in $\Xi^*(h)$. Hence, this domain is called adiabatic chaos area (on the level $H_W = h$).

The Poincaré mapping can be used to study the solutions' properties in $\Xi^*(h)$. After the canonical transformation (2.2) is performed, the values of the variables $\overline{x}, \overline{\chi}$ at the phase trajectory successive transitions through the plane $\overline{y} = 0$ with $\dot{\overline{y}} > 0$ (i.e., at the transitions from the region $\overline{y} < 0$ to the region $\overline{y} > 0$) are connected through

$$\overline{\chi}_{k+1} = V(\overline{\chi}_k, \overline{x}_k, h),\ \overline{x}_{k+1} = U(\overline{\chi}_k, \overline{x}_k, h), \tag{4.1}$$

where h defines the level of H_W.

We construct the Poincaré mapping numerically. It turns out that, instead of the variables $\overline{\chi}, \overline{I}, \overline{x}, \overline{y}$, it is convenient to introduce the variables $\widehat{\chi}, \widehat{I}, \widehat{x}, \widehat{y}$ connected to the original variables φ, Φ, x, y by means of more simple formulae

$$\widehat{\chi} = \chi(\varphi, \Phi, x, y),\ \widehat{I} = I(\varphi, \Phi, x, y), \tag{4.2}$$

$$\widehat{x} = x + \varepsilon \frac{\partial W}{\partial y}(\varphi, \Phi, x, y),\ \widehat{y} = y - \varepsilon \frac{\partial W}{\partial x}(\varphi, \Phi, x, y).$$

To calculate the derivatives $\partial W/\partial x, \partial W/\partial y$ we use the relations obtained in [5]:

$$\frac{\partial W}{\partial \xi} = \frac{1}{\sigma\omega(\kappa)} \int_0^{\widehat{\chi}} \left(\frac{\partial H_W}{\partial \xi} - \left\langle \frac{\partial H_W}{\partial \xi} \right\rangle \right) d\chi =$$

$$= \frac{1}{\sigma\omega(\kappa)} \int_0^{\widehat{\chi}} \left\{ \left(\frac{\partial A}{\partial \xi} \right) [\cos(\varphi - R) - \langle \cos(\varphi - R) \rangle] - \right.$$

$$\left. - A \left(\frac{\partial R}{\partial \xi} \right) \sin(\varphi - R) \right\} d\chi,\ \xi = x, y.$$

Here $\omega(\kappa)$ denotes the frequency of the motion in the fast subsystem:

$$\omega(\kappa) = \begin{cases} \dfrac{\pi\kappa\sqrt{\alpha A}}{K\left(\dfrac{1}{\kappa}\right)}, & \kappa > 1 \\ \\ \dfrac{\pi\sqrt{\alpha A}}{2K(\kappa)}, & \kappa < 1 \end{cases}$$

In fact, the difference between the non-canonical change of variables

$$(\varphi, \Phi, x, y) \to (\widehat{\chi}, \widehat{I}, \widehat{x}, \widehat{y})$$

and the canonical transformation (2.2) is small enough:

$$|\overline{\chi} - \widehat{\chi}| = O(\varepsilon),\ |\overline{I} - \widehat{I}| = O(\varepsilon),$$

$$|\overline{x} - \widehat{x}| = O(\varepsilon^2),\ |\overline{y} - \widehat{y}| = O(\varepsilon^2)$$

in every point in the region where both these sets of variables are defined.

As an example, the points at which two regular and one chaotic trajectories cross the hyperplane $\widehat{y} = 0$ (passing from the region $\widehat{y} < 0$ to the region $\widehat{y} > 0$) are shown in Fig. 15. Fig. 16 demonstrates the existence of the stability island filled with invariant curves in the chaotic region of the mapping

$$\widehat{\chi}_{k+1} = \widehat{V}(\widehat{\chi}_k, \widehat{x}_k, h),\ \widehat{x}_{k+1} = \widehat{U}(\widehat{\chi}_k, \widehat{x}_k, h). \tag{4.3}$$

Stable fixed point in the center of Fig. 16 corresponds to the stable periodic solution of the equations (1.1) embedded into the adiabatic chaos area $\Xi^*(h)$. Taking into account the typical time between two successive passages of the phase point through the plane $\widehat{y} = 0$, we can estimate the period of this solution as $O\left(\frac{1}{\varepsilon}\right)$. So it is reasonable to specify it as a long-periodic solution.

As it was established in [6], in the case of the Hamiltonian system with one degree of freedom depending on slowly varying parameter, the number of stability islands located inside the adiabatic chaos area is large enough and is of order $\sim 1/\varepsilon$. Moreover, the total measure of these islands on the Poincaré section is comparable with the measure of the chaotic area as a whole. Although the Wisdom system has two degrees of freedom, on the level H_W it can be reduced to the Hamiltonian system of the lower dimension with a time-dependent parameter. So it is natural to expect the existence of many stable periodic solutions with the periods $\sim 1/\varepsilon$ inside $\Xi^*(h)$. This is confirmed by the numeric results presented in **Sec. 4.2**. In [15] it is proven rigorously that the Hamiltonian system with two degrees of freedom indeed can possess the numerous stable periodic solutions lying in the adiabatic-chaos realm.

Note. Except the adiabatic-chaos area $\Xi^*(h)$ the Wisdom system has an area of the so-called homoclinic chaos [12]. An interaction of the fast and slow subsystems results in the splitting of the separatrices which constitute closed contours on the slow-motion phase portraits constructed in the adiabatic approximation (**Sec. 3**). The width of the emerging stochastic layer can be estimated as $O\left(\exp(-C_1/\varepsilon)\right)$, where C_1 is some positive constant [16, 17]. The dynamics in this region of the system's phase space is beyond the scope of our current study.

4.2. Numeric search of the stable long-periodic solutions inside the adiabatic chaos region

As an example, we evaluate numerically the amount of the stable periodic solutions in $\Xi^*(h)$ at $h = 1.9$. In this case the adiabatic-chaos area consists of two components, Ξ_1^* and Ξ_2^* (Fig. 14). To simplify the computations, we consider the "symmetric" periodic solutions solely. "Symmetric" is a solution satisfying the conditions

$$\varphi(0) = 0 \bmod \pi, \ \varphi\left(\frac{T}{2}\right) = 0 \bmod \pi, \tag{4.4}$$

$$y(0) = y\left(\frac{T}{2}\right) = 0,$$

for a certain $T > 0$. Taking into account the Wisdom system's reversibility (**Sec. 1**), one can prove that any solution of the boundary value problem

(4.4), being extended outside the interval $[0, \frac{T}{2}]$, gives birth to a T-periodic solution of equations (1.1) with the monodromy matrix

$$M(h) = QW^{-1}\left(\frac{T}{2}, h\right) QW\left(\frac{T}{2}, h\right).$$

Here $W(t,h)$ denotes the fundamental matrix of the appropriate linearised equations ($W(0,h) = E_4$, where E_4 is the (4×4)-identity matrix).

Since there are no reasons to assume that only "symmetric" stable periodic solutions are accepted by the Wisdom system, the results of our calculations should be interpreted as the lower bound estimations.

To select the stable solutions, we undertake the usual analysis restricted by the linear approximation. The characteristic equation

$$\det\left(M(h) - \rho E_4\right) = 0$$

can be rewritten as

$$(\rho - 1)^2(\rho^2 - 2a\rho + 1) = 0,$$

where

$$a = \frac{\mathrm{tr}\, M}{2} - 1.$$

The solution $\mathbf{z}(t)$ is stable at $|a| < 1$.

Table 2. Numerically found stable periodic solutions satisfying conditions (4.4)

ε	The number of solutions in Ξ_1^*	The number of solutions in Ξ_2^*	The total number of solutions
0.2	4	4	8
0.1	18	24	42
0.05	37	37	74
0.025	72	63	135

Information about the stable periodic solutions found numerically in $\Xi^*(h)$ can be found in Table 2. The amount of such solutions N increases as the parameter ε decreases.

It would be important to mention that the existence of numerous stable periodic solutions inside the adiabatic-chaos area was proven in [6, 15] under the assumption of $\varepsilon^{1/3} \ll 1$. This assertion is not valid for the values of ε used in our numerical study. (Our computer facilities were too week for an extensive search of periodic solutions at $\varepsilon < 0.025$). Nevertheless, the derived in [6] asymptotic relation $N \sim 1/\varepsilon$ was satisfied, with a reasonable accuracy, even at $\varepsilon \leq 0.1$ (Fig. 17).

Conclusion

We present a number of patterns in the slow motion behavior in the Wisdom system. However, our results can be applied to the analysis of the asteroidal resonant motion only when this system is an adequate model. In general it misses some significant features of the original three body problem. For example, the Wisdom system can not be used to study an interplay of low- and high-eccentricity motions at the 3:1 resonance described in [7]. It reveals the necessity of examining the exactness of the Wisdom model in this context.

According to [6, 15], the existence of many stable periodic solutions is a rather general property of the adiabatic chaos area in the phase space of Hamiltonian systems. Our numerical quest for periodic solutions in Wisdom system confirms this conjecture.

Acknowledgements

We thank M.Efroimsky and A.Vasiliev for reading through this paper before publications and suggesting some improvements. Our work was supported by Russian Foundation for Basic Researches via Grants 03-01-00158, NSh-136.2003.1, and NSh-2003.2003.1. AIN acknowledges the support from the "Integration" Program via Grant B0053.

References

[1] J.Wisdom, The origin of the Kirkwood gaps: a mapping for the asteroidal motion near the 3/1 commensurability, *Astr. J.*, **87** (1982), 577-593.

[2] J.Wisdom, Chaotic behavior and the origin of the 3/1 Kirkwood gap, *ICARUS*, **56** (1983), 51-74.

[3] J.Wisdom, A perturbative treatment of motion near the 3/1 commensurability, *ICARUS*, **63** (1985), 272-286.

[4] A.I.Neishtadt, Jumps of the adiabatic invariant on crossing the separatrix and the origin of the 3:1 Kirkwood gap, *Dokl. Akad. Nauk SSSR*, **295** (1987), 47-50 (Russian). English transl.: *Sov. Phys. Dokl.*, **32** (1987), 571-573.

[5] A.I.Neishtadt, Change of an adiabatic invariant at a separatrix in the systems with two degrees of freedom, *Prikl. Mat. Mekh.*, **51** (1987), 750-757 (Russian). English transl.: *PMM USSR*, **51** (1987), 586-592.

[6] A.I.Neishtadt, D.V.Treschev, V.V.Sidorenko, Stable periodic motions in the problem of passage through a separatrix, *CHAOS*, **7** (1997), 2-11.

[7] S.Ferraz-Mello, J.C.Klafke, A model for the study of very-high-eccentricity asteroidal motion. The 3:1 resonance. In *Predictability, Stability and Chaos in N-body Dynamical Systems (A.E.Roy, ed.)*, Plenum Press, New York (1991), 177-184.

[8] J.D.Hadjidemetriou, The elliptic restricted problem at the 3:1 resonance, *Celest. Mech. Dyn. Astron.*, **53** (1992), 151-183.

[9] J.Henrard, N.D.Caranicolas, Motion near the 3/1 resonance of the planar elliptic restricted three body problem, *Celest. Mech. Dyn. Astron.*, **47** (1990), 99-121.

[10] G.W.Hill, Illustrations of periodic solutions in the problem of three bodies, *Astr. J.*, **22** (1902), 117-121.

[11] A.T.Sinclair, Periodic solutions close to commensurabilities in the three body problem, *Mon. Not. Roy. Astr. Soc.*, **148** (1970), 325-351.

[12] J.Koiller, J.M.Balthazar, T.Yokoyama, Relaxation-chaos phenomena in celestial mechanics, *Physica D*, **26** (1987), 85-122.

[13] J.D.Hadjidemetriou, Asteroid motion near the 3:1 resonance, *Celest. Mech. Dyn. Astron.*, **56** (1993), 563-599.

[14] F.Varadi, W.M.Kaula, Chaos in the 3:1 mean-motion resonance revisited, *Planet. Space Sci.*, **47** (1999), 997-1003.

[15] A.I.Neishtadt, D.V.Treschev, A.A.Vasiliev *(in preparation)*.

[16] A.I.Neishtadt, The separation of motions in the systems with rapidly rotating phase, *Prikl. Mat. Mekh.*, **48** (1984), 197-204 (Russian). English transl.:*J. Appl. Math. Mech.*, **48** (1984), 133-139.

[17] A.Delshams, V.Gelfreich, A.Jorba, T.M.Seara, Exponentially small splitting of separatrices under fast quasiperiodic forcing, *Comm. Math. Phys.*, **189** (1997), 35-71.

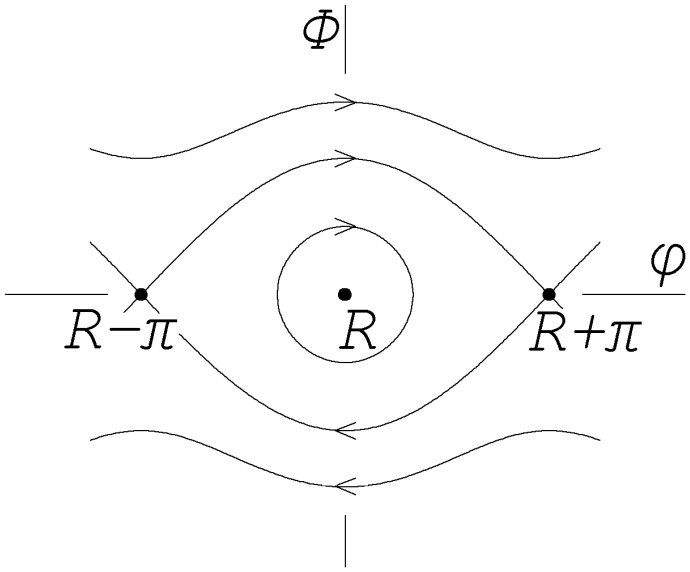

Fig.1. The phase portrait of the fast subsystem at $\varepsilon = 0$

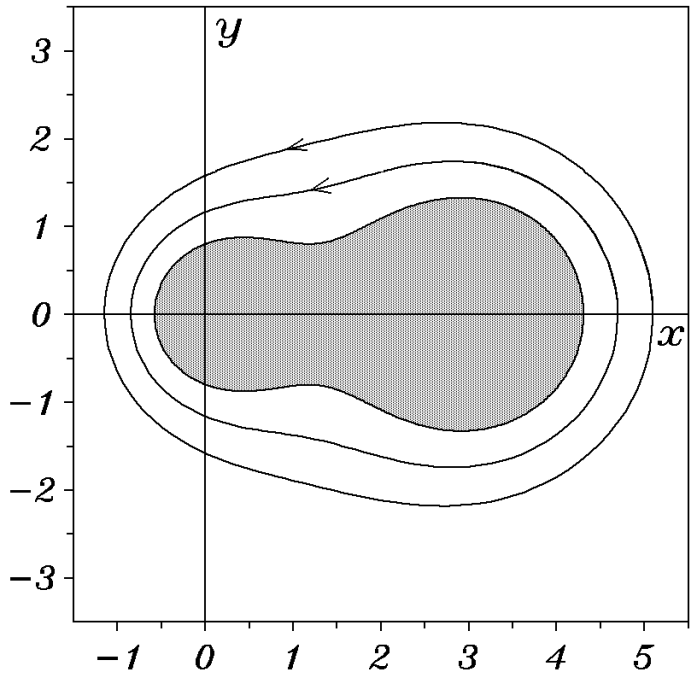

Fig.2. The slow motions at $h = -2$ (Type I phase portrait). The forbidden area is shaded.

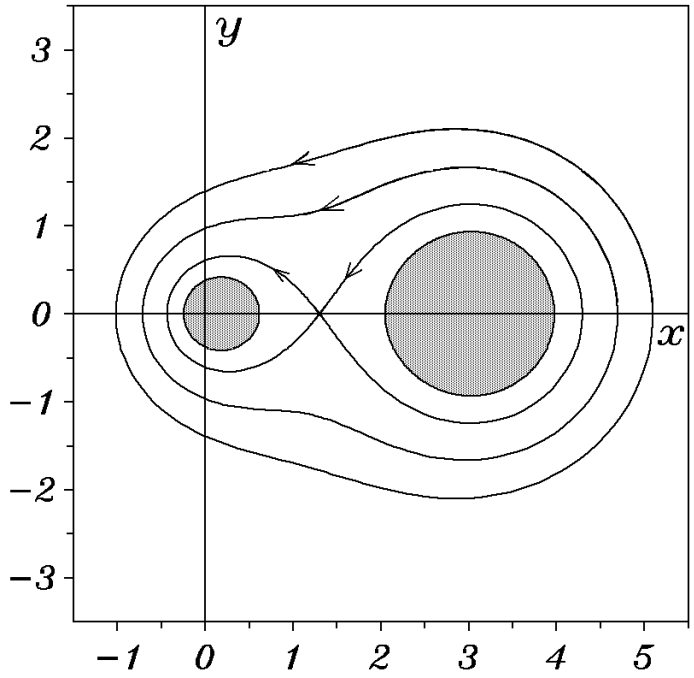

Fig.3. The slow motions at $h = -1$ (Type II phase portrait). The forbidden area is shaded.

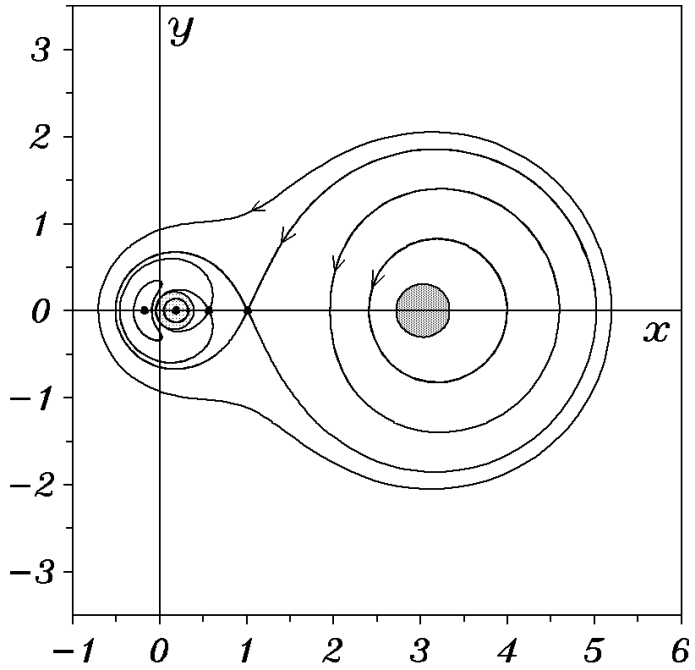

Fig.4. The slow motions at $h = 0.5$ (Type III phase portrait). The more shaded domain is the forbidden area (right). The less shaded domain is the part of the slow variables plane enclosed by the uncertainty curve $\Gamma(h)$ (left).

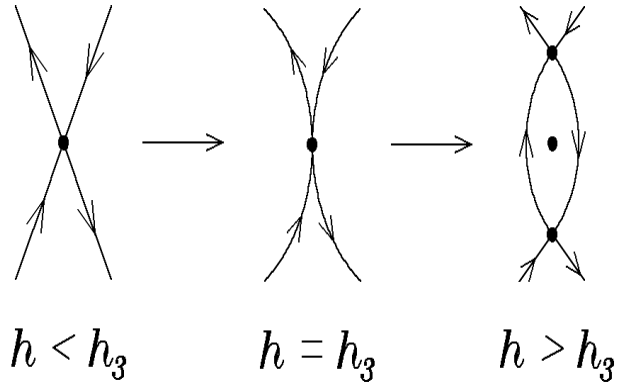

Fig.5. The bifurcation of the phase portrait at $h = h_3$

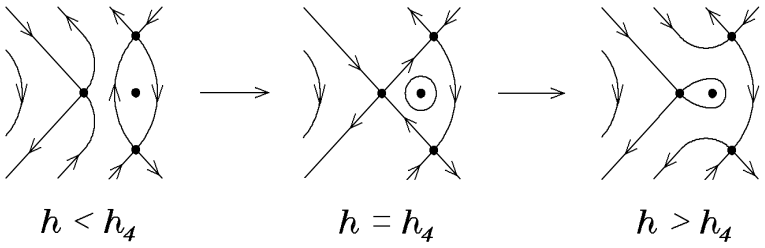

Fig.6. The bifurcation of the phase portrait at $h = h_4$

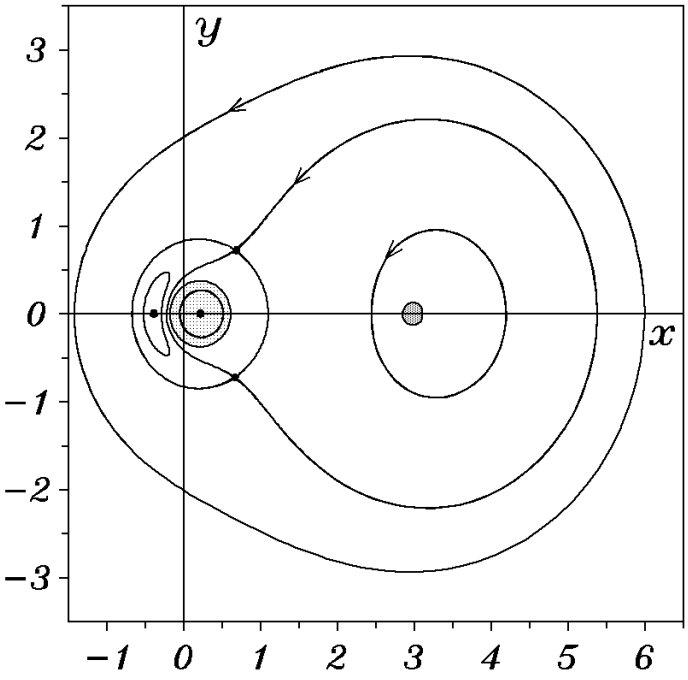

Fig.7. The slow motions at $h = 0.9$ (Type VI phase portrait). The more shaded domain is the forbidden area (right). The less shaded domain is the part of the slow variables plane enclosed by the uncertainty curve $\Gamma(h)$ (left).

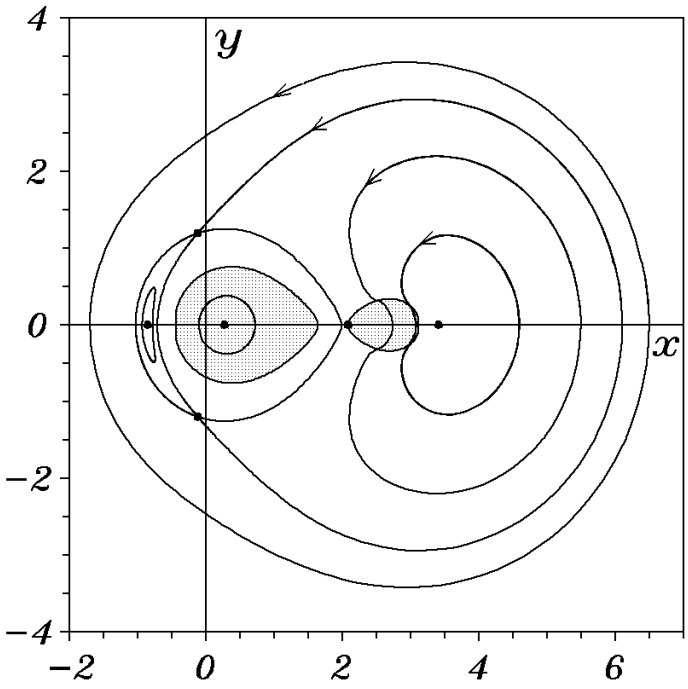

Fig.8. The slow motions at $h = 1.9$ (Type VII phase portrait). The shaded domains are the parts of the slow variables plane enclosed by the uncertianty curve $\Gamma(h)$.

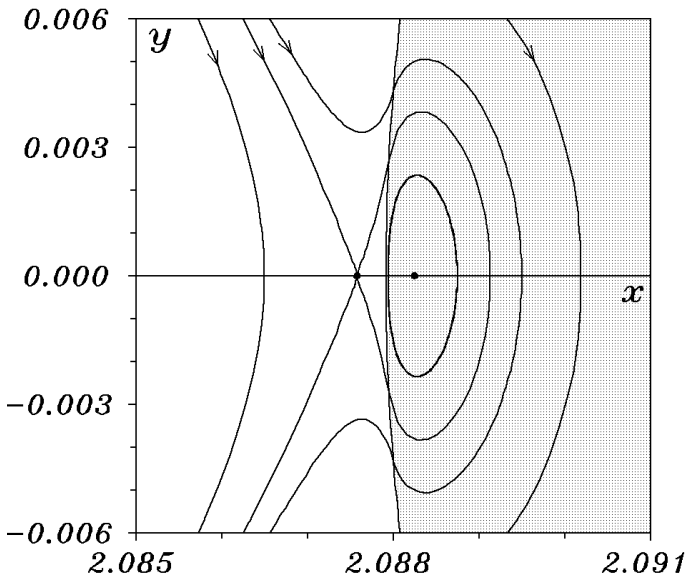

Fig.9. The enlarged fragment of the phase portrait at $h = 1.9$. The equilibria located in the close vicinity of the uncertainty curve are shown.

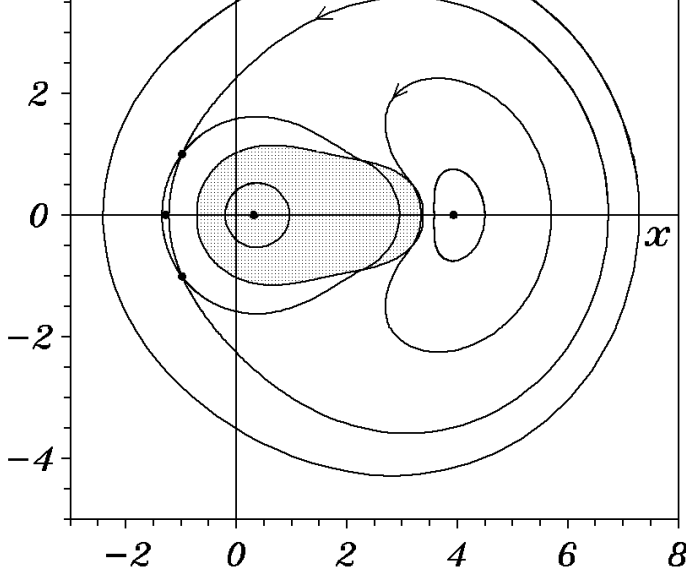

Fig. 10. The slow motions at $h = 3.0$ (the type VIII phase portrait). The shaded domain is the part of slow variables plane enclosed by $\Gamma(h)$.

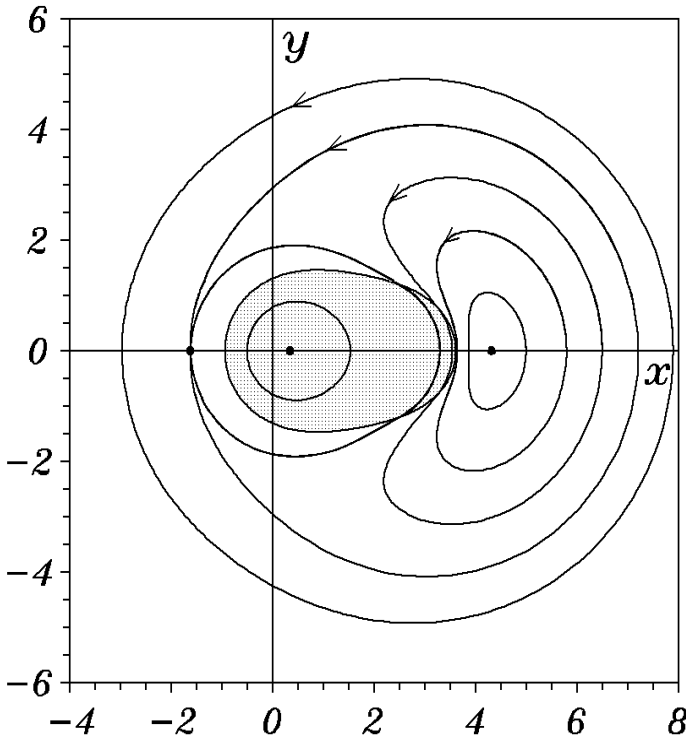

Fig. 11. The slow motions at $h = 4.0$ (the type IX phase portrait). The shaded domain is the part of slow variables plane enclosed by $\Gamma(h)$.

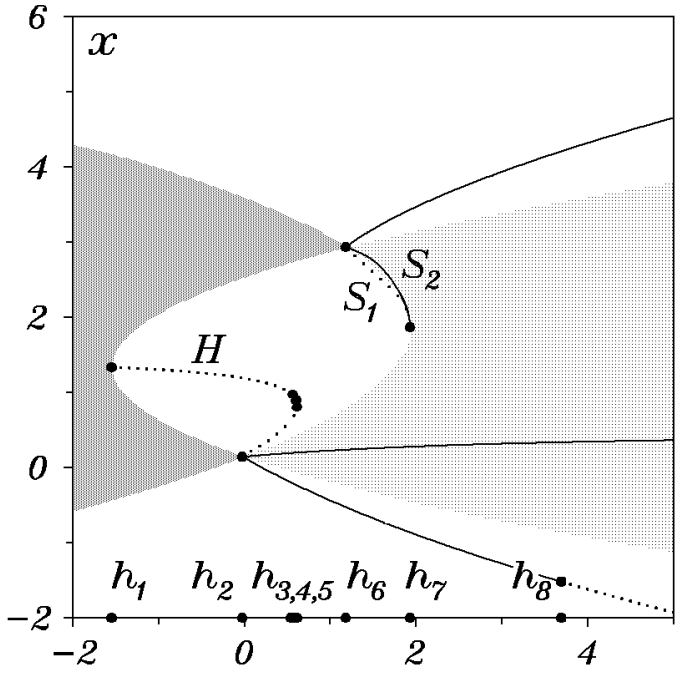

Fig. 12. Bifurcation diagram: location of the system (2.9) equilibria on the Ox axis. Solid lines correspond to stable equilibria, dotted lines represent unstable ones. More and less shaded domains provide an idea about the location of the forbidden area $M(h)$ and the uncertainty curve $\Gamma(h)$ respectively. Namely, the vertical segments of the more shaded domain represent the segments of the Ox axis lying inside $M(h)$ at corresponding value of h. In the similar way the less shaded domain represents the segments of the Ox axis inside the areas enclosed by $\Gamma(h)$.

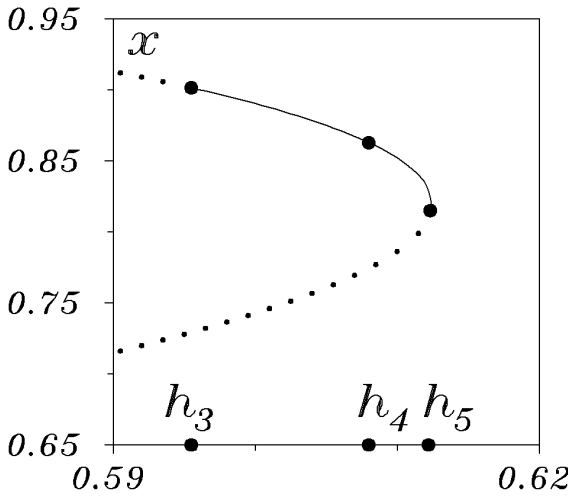

Fig. 13. The enlarged fragment of the bifurcation diagram

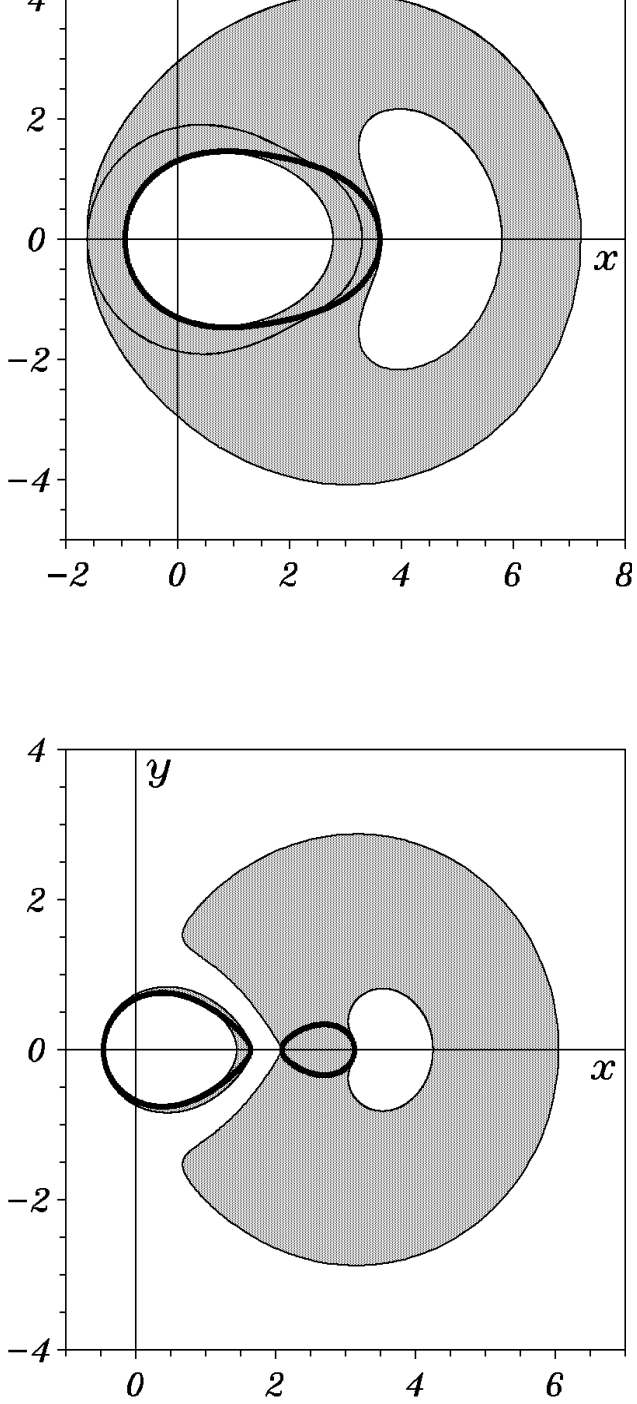

Fig. 14. The adiabatic chaos regions (shaded) on the slow variables plane at $h = 1.9$ (top) and $h = 4.0$ (bottom). The thick lines are used to show the uncertainty curve location.

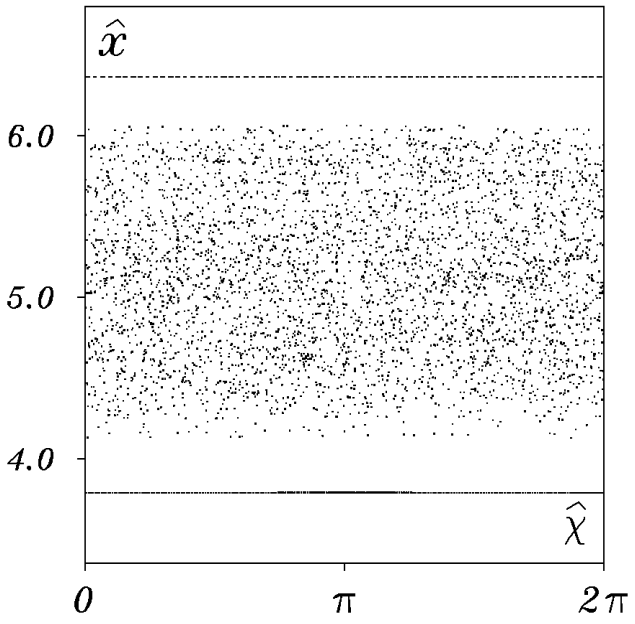

Fig. 15. Poincaré section of the system's phase flow on the level $h = 1.9$. Two regular and one chaotic (embedded into $\Xi^*(h)$) trajectories are shown.

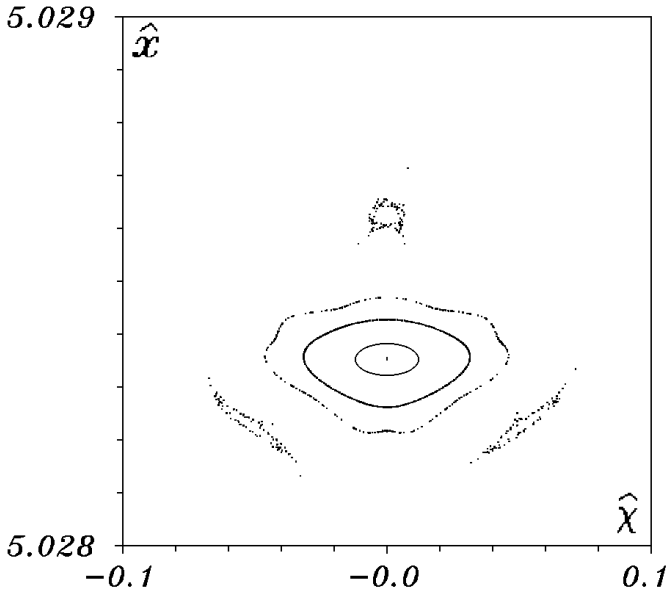

Fig. 16. An example of the stability island in the adiabatic chaos region ($h = 1.9$)

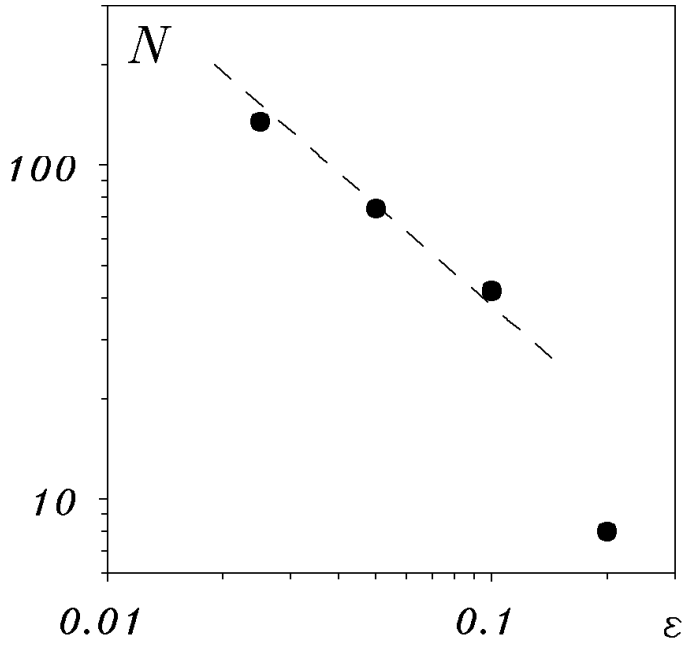

Fig. 17. The amount of the numerically found stable periodic solutions at different values of parameter ε. The dashed line is the graph of the function $N = c/\varepsilon$, $c = 3.8$.